



Interrelation Among Morphology, Mechanical Properties and Oxidation Behavior of $\text{Nb}_x\text{Al}_y\text{N}_z$ Thin Films

Renata Gomes Carvalho^{a*}, Daniel Angel Ramirez Fernandez^a, Vagner Fontes Dória Soares^a,
Frederico Guilherme Carvalho Cunha^a, Fabiana Magalhães Teixeira Mendes^b, Roberto Hübler^c,
Giovanna Machado^d, Eduardo Kirinus Tentardini^a

^aUniversidade Federal de Sergipe, Av. Marechal Rondon, S/N, São Cristóvão, SE, Brasil

^bInstituto Nacional de Tecnologia, Av. Venezuela, 82, Rio de Janeiro, RJ, Brasil

^cPontifícia Universidade Católica do Rio Grande do Sul - PUC-RS, Av. Ipiranga, 6681,
Porto Alegre, RS, Brasil

^dCentro de Tecnologia Estratégicas do Nordeste, Recife, PE, Brasil

Received: April 17, 2019; Revised: August 12, 2019; Accepted: September 18, 2019

$\text{Nb}_x\text{Al}_y\text{N}_z$ thin films were deposited by magnetron sputtering reactive technique with $(y/x+y)$ ratio varying from 0 to 0.4, in order to maintain aluminum atoms inside NbN matrix in solid solution. GAXRD analyses revealed that the crystalline phase obtained for $\text{Nb}_x\text{Al}_y\text{N}_z$ thin films was B1-NbN with a lattice constant shrinkage as Al concentration at these coatings was verified. Due to similarity in electro negativity values between Nb and Al, XPS analyses could not verify pronounced changes among as deposited $\text{Nb}_x\text{Al}_y\text{N}_z$ coatings. The average hardness values evidenced that solid solution strengthening mechanism did not increase hardness significantly. The oxidation resistance increased with Al content and no oxide phases were registered by GAXRD analyses for coating with more aluminum added. However, SEM images revealed bubbles after oxidation at high temperatures for all samples.

Keywords: thin films, magnetron sputtering, niobium nitride, aluminum nitride, NbAlN, high temperature oxidation.

1. Introduction

Niobium nitride (NbN) has been widely explored as protective coatings mainly due to properties such as high hardness and wear resistance, providing an interesting option for applications that require good mechanical performance^{1,2}. Initially, NbN was used as a component in multilayered thin films along with titanium nitride (TiN)³⁻⁵, showing significant improvements regarding hardness and corrosion resistance. Remarkably, when the two nitrides were analyzed separately in those works, NbN showed higher hardness and wear resistance values compared to TiN.

Despite the good mechanical properties, oxidation temperature of NbN is near to 700 K⁶, which compromises its applicability in high temperature service conditions. One possibility to hinder NbN oxidation process is the addition of a third chemical element, in its matrix, such as aluminum. Al atoms have already been successfully incorporated in Ti(Al)N, Cr(Al)N, Zr(Al)N and Ta(Al)N thin films, improving the oxidation resistance besides good results in coatings mechanical properties⁷⁻¹¹. However, as seen in the literature, adding a different element or molecule to coatings matrixes is highly prone to result in strong changes on the formed

structure and properties¹². In particular, when aluminum solubility limit is exceeded, hexagonal AlN phase (B4-AlN) is commonly formed, rendering the ternary coating an improved oxidation resistance but strongly decreasing global mechanical resistance^{7,13,14}, suggesting the best results for thermal stability and mechanical properties for these nitrides are obtained when aluminum atoms are exclusively in solid solution, without hexagonal AlN grains formation^{13,14}.

Notably, Al solubility in NbN matrix has been reported to be highly dependent on the formed structure. It is relevant to the formation of ternary $\text{Nb}_x\text{Al}_y\text{N}_z$, given the numerous crystalline structures that pure NbN can manifest, i.e., hexagonal β -Nb₂N, δ' -NbN, ϵ -NbN and fcc δ -NbN. Earlier works have demonstrated that the latter can accommodate more Al atoms in solid solution compared to the others NbN crystalline structures, retarding therefore B4-AlN or transitions phases formation in $\text{Nb}_x\text{Al}_y\text{N}_z$ with $(y/x+y)$ ratio value up to 0.45^{14,15}. Thus, a few works reported the thermal stability and tribological behavior for NbAlN cubic structure (B1 phase) with Al in solid solution¹⁴⁻¹⁷, however none systematically concerning the influence of aluminum content in B1-NbAlN on crystalline structure, chemical bonds, hardness and oxidation at high temperatures.

*e-mail: renatacarvalho.rc@gmail.com

Hence, the present work aims to investigate how the morphological and structural characteristics impact hardness and oxidation resistance of $\text{Nb}_x\text{Al}_y\text{N}_z$ thin films with rock-salt cubic structure, as well as pure NbN and AlN coatings for comparative analyses. Coatings were characterized by Rutherford Backscattering Spectrometry (RBS), Glancing Angle X-ray Diffraction (GAXRD), X-ray photoelectron spectroscopy (XPS), nanohardness, oxidation tests at temperatures up to 873 K and Scanning Electron Microscope (SEM).

2. Material and Methods

Coatings were deposited by reactive magnetron sputtering with an AJA Orion equipment 5-HV Sputtering Systems model. Niobium and aluminum targets with purity of 99.99% were applied on RF and DC power supply, respectively. Polyethylene and silicon wafer substrates used were subjected to ultrasonic bath for 20 minutes with distilled water and detergent and then dried. Furthermore, the silicon substrates were subjected to a bath in hydrofluoric acid solution to remove oxides existing on the surface.

For $\text{Nb}_x\text{Al}_y\text{N}_z$ coatings all deposition parameters were kept constant, except for the Al target power which was varied to achieve different aluminum concentrations. Additionally, pure NbN and AlN coatings were deposited with the same basic parameters of $\text{Nb}_x\text{Al}_y\text{N}_z$ coatings, but using only one target at a time. Prior to nitrides deposition, an interlayer of Nb for NbN and $\text{Nb}_x\text{Al}_y\text{N}_z$ samples and Al for AlN samples were deposited for 5 min. All main deposition parameters can be seen in Table 1.

RBS analysis were performed using a 3 MV Tandemron with alpha particles accelerated up to 2 MeV, with a silicon based detector at an angle of 165° and resolution of 12 keV. The GAXRD analyses were executed on a Shimadzu LabX XRD-6000 model (Cu-K α radiation; $\lambda = 1.54 \text{ \AA}$) with grazing angle of 1° ; scan speed = $2^\circ/\text{min}$; fixed time; voltage = 40 kV; current = 30 mA. Measurement values were obtained at 2θ from 20° to 80° and peaks were identified by comparison with International Centre for Diffraction Data (ICSD) data files.

XPS was recorded using a hemispherical spectrometer PHOIBOS 150- SPECS equipped with X-Ray Gun (XR-50) with an Al K α source (soft X-ray source at 1486.6 eV, which

is non-monochromatic). The base pressure in the analysis chamber was about 10^{-8} Pa. The anode was operated at 10 W (10 kV, 10 mA) and the analyzer was operated at constant pass energy of 50 eV for survey spectra and 20 eV for selected regions. Before analyzes, all samples were subjected to surface cleaning with Ar^+ (1.0 KeV) sputtering procedure for 10 minutes. The ion source IQE12/38 from SPECS was used, which allows the operation at 5 KeV beam energy. The incidence angle is preselected to be 50° , as the sample was not tilted (rotation angle at 0°). The binding energy shifts due to surface charging were corrected using the C 1s level at 284.6 eV, as an internal standard. The spectra were Shirley background-subtracted across the energy region and fitted using CasaXPS Version 2.3.15.

Hardness values were obtained through nanoindentation tests in a Fisherscope HV 100 with a Berkovich indenter. It was performed ten indentations for each analysis, with depth of 40 nm, 10 mN load and 60 seconds for indentation. Oxidation tests on NbN, AlN and $\text{Nb}_x\text{Al}_y\text{N}_z$ coatings were conducted in a traditional electrical resistance furnace. Samples were annealed in ambient atmosphere at 773 and 873 K for 30 minutes. Thereafter, samples were analyzed again by GAXRD and nanohardness tests using the same parameters mentioned above. Surface morphology after oxidation tests was analyzed by SEM using a JEOL JCM 5700 microscope.

3. Results and Discussion

3.1 Composition characterization

$\text{Nb}_x\text{Al}_y\text{N}_z$ samples were analyzed by RBS in order to precisely determine chemical composition of the coatings. A typical RBS spectrum is shown in Figure 1, obtained from pure NbN and $\text{Nb}_{0.28}\text{Al}_{0.19}\text{O}_{0.05}\text{N}_{0.48}$ samples. Polyethylene substrates were employed for RBS analyses aiming to eliminate high background signal from the silicon wafer used in the present work for other characterizations. Similar spectra (not shown) were obtained for other $\text{Nb}_x\text{Al}_y\text{N}_z$ samples.

Additionally to the presence of aluminum peak, another noticeable difference between both spectra is the width and intensity in niobium and nitrogen peaks, respectively. The first fact is attributed to the increased thickness associated with aluminum incorporation, given that all parameters

Table 1. Main deposition parameters for NbN, AlN and $\text{Nb}_x\text{Al}_y\text{N}_z$ coatings.

RF power applied to Nb target (W/cm^2) (NbN, NbAlN_10, NbAlN_20 and NbAlN_40)	7.6
DC power applied to Al target (W/cm^2)	AlN=7.6; NbAN_10=0.5; NbAlN_20=3.0; NbAlN_40=5.0
Base Pressure (Pa)	1×10^{-5}
Working Pressure (Pa)	3×10^{-1}
Flow rates (scm)	Ar=14; $\text{N}_2=7$
Deposition parameters niobium interlayer (NbN, NbAlN_10, NbAlN_20 and NbAlN_40)	2 min; 3×10^{-1} Pa; 100% Ar; 20 scm; 7.6 W

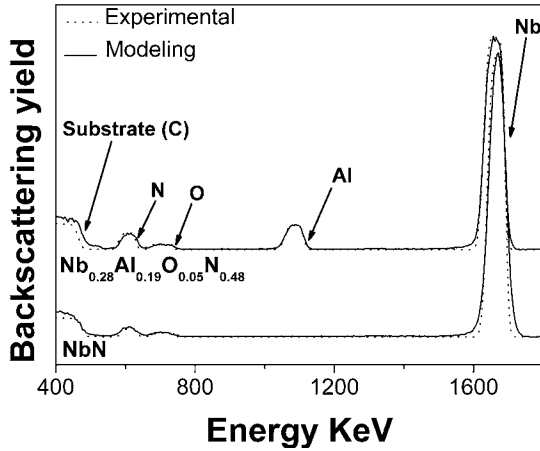


Figure 1. RBS result for the NbN and Nb_{0.28}Al_{0.19}O_{0.05}N_{0.48} samples.

regarding NbN were kept constant in all samples. The latter is related to nitrogen raised concentration due to establishment of Al - N bonds.

Using computational simulation software X-rump it was possible to estimate the variation of aluminum concentration for RBS spectra. Table 2 shows the chemical composition obtained for all samples, which nomenclatures are based on Al/(Nb+Al) ratio. Oxygen detected in the samples can be explained as a contaminant derived from reactions between Nb and residual O₂/H₂O molecules adsorbed in the chamber, though similar oxygen concentrations are frequently found for nitrides deposited by reactive magnetron sputtering^{14,15,17}.

3.2. Structure analysis

GAXRD obtained from as deposited AlN, NbN, NbAlN₁₀, NbAlN₂₀ and NbAlN₄₀ samples are shown in Figure 2. AlN sample showed a hexagonal wurtzite B4 (JCPDS 65 - 1902) structure while NbN presented a cubic rock-salt B1 (JCPDS 38 - 1155). Nb_xAl_yN_z patterns maintained NbN peaks, with no AlN phase identified. The peak at 38.2° is related to the BCC niobium phase from Nb interlayer primarily deposited for all Nb_xAl_yN_z samples (JCPDS 35 - 789). The Al interlayer peak was also observed on AlN diffractogram at 44.6° (JCPDS 4 - 787).

Aluminum atoms addition in the ternary nitride coatings promoted a shift of all NbN peaks to larger angles regions, suggesting an interplanar distance shrinkage, from 4.38 Å for pure NbN to 4.28 Å for NbAlN₄₀ sample. Such fact is

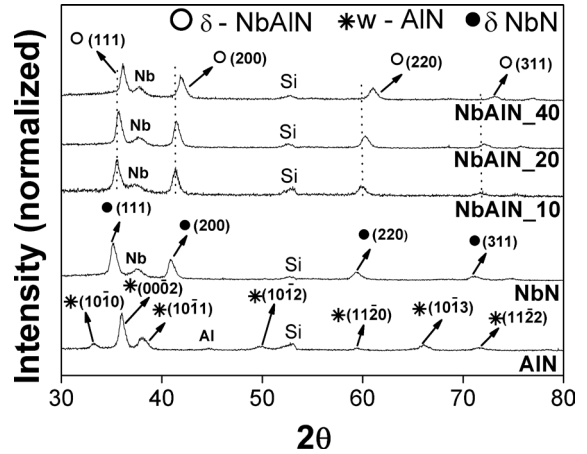


Figure 2. XRD patterns for AlN, NbN and Nb_xAl_yN_z samples as deposited.

related to the substitution of Nb by Al atoms, since aluminum possess a smaller ionic radius compared to niobium, 0.54 Å and 0.72 Å, respectively¹⁸.

The average crystallite size was estimated by Debye-Scherrer equation using the FWHM value from XRD diffraction peaks. The values for samples NbN, NbAlN₁₀ and NbAlN₂₀ were basically the same, varying from 11.7 nm to 11.1 nm. However, for NbAlN₄₀ the calculated crystallite size value was 13.1 nm, which is greater than pure NbN and reveals a higher degree of crystallinity when compared to other percentages.

In contrast, it is interesting to observe that this last sample presented a broadening in (200) peak. According to literature¹⁹, at Al/(Nb+Al) ratio value close to 0.45, NbAlN cubic structure transforms into hexagonal B_k phase, which represents the transition between B1 and B4 phases and possess a similar formation energy to the cubic NbAlN structure. Thus, such broadening probably indicates the start point in a tendency to form the B_k transition phase. That fact, associated with the strong shift of B1-NbN peaks to higher angles, suggests that in sample NbAlN₄₀ the aluminum addition induced the disorder of original NbN cubic structure more intensively in order to better accommodate aluminum atoms. In other words, although the highest percentage of Al atoms resulted in the increased grain size for plane (111), the solid solution NbAlN with 40 at.% Al is probably close to its solubility limit.

Table 2. RBS results with the composition of the deposited films on polyethylene substrate

Sample	Nb (at.%)	Al (at.%)	N (at.%)	O (at.%)	(Al/(Nb+Al))*100
NbN	47.6	-	47.6	4.8	-
NbAlN ₁₀	40.6	4.9	49.6	4.9	10.7
NbAlN ₂₀	37.2	9.7	48.3	4.8	20.6
NbAlN ₄₀	28.6	19.1	47.6	4.7	40.0

For a better understanding of the formed structures, XPS analyses were performed and core-level spectra of Nb 3d, Al 2p and N 1s regions from NbN, AlN and $Nb_xAl_yN_z$ samples are shown in Figure 3a, 3b and 3c, respectively. Sample NbAlN_20 spectra for all regions presented very similar results compared to NbAlN_40 sample and, for better spectra visualization, these analyses will not be shown.

Figure 3a shows Nb 3d photoelectron region from NbN, NbAlN_10 and NbAlN_40. The best fit deconvolution yielded three doublets, the component with lower binding energy (203.3 - 206.8 eV) was attributed to Nb 3d_{5/2} - Nb 3d_{3/2} electrons of NbN compound^{19,20}. The doublet component at binding energy 204.0 eV (Nb 3d_{3/2}) was assigned to Nb-O-N oxynitrides^{17,20,21}. It could also be identified a small contribution from Nb-O oxide phases at 206 eV for Nb 3d_{5/2} and 208.8 eV for Nb 3d_{3/2}^{20,22,23}. These results are in agreement with previous works^{17,24}, where oxide compounds are commonly identified in sputtered thin films, and has also been found in RBS analyses. No significant binding energy shift was observed in this region as the Al concentration was raised.

The best fit from N 1s region for AlN, NbN, NbAlN_10 and NbAlN_40 samples is shown in Figure 3b. From AlN sample, N 1s spectrum was deconvoluted into two peaks. Peaks identified at 396.3 eV and 397.7 eV were attributed to AlN and Al-O-N oxynitride compounds, respectively^{25,26}. The core-level spectra from NbN sample yielded two peaks at 396.7 and 397.4 eV, attributed to NbN compounds and Nb-O-N oxynitride presence.

The NbAlN_10 core-level spectra showed a peak centered at 396.9 eV, associated to NbN compounds, a peak at 396.3 eV attributed to Al-N bond^{17,24}, and a weak peak centered at 397.6 identified as Nb-O-N oxynitride compounds^{17,27}. From NbAlN_40 sample, the N 1s spectrum revealed the presence of characteristic peaks of NbN (396.7 eV) and AlN (395.9 eV) nitrides, in addition to oxynitride presence (397.4 eV). It is possible to observe a tendency of reduction on energy values attributed to Al-N bonds with the increase of aluminum concentration. However, this displacement is lower than 0.5 eV, thus it is not possible to ensure a significant change. From Holec *et al.*²⁸, the charge transfer in a solid solution formed by $Nb_xAl_yN_z$ with cubic structure presents a greater dispersion for N atoms. The charger transfer is larger from Al to N than from Nb to N, which suggest that the Al-N bond is more ionic than Nb-N one.

In parallel, Al 2p spectrum of AlN and NbAlN_40 samples (Figure 3c) showed a peak at a binding energy of 73.4 eV, that could be assigned to AlN compounds^{17,29-31}. Due to the high background noise caused by low aluminum concentration, the spectrum obtained for samples NbAlN_10 and NbAlN_20 will not be shown. No significant binding energy shift was observed between pure AlN and NbAlN_40 samples. The best fit deconvolution of this band also indicated the presence of a weak peak centered at 74.3 eV, which was attributed to the presence of aluminum oxides^{29,31,32}.

From Nb 3d and Al 2p regions it is possible to suggest that the electronic surroundings of both atoms is not affected by the presence of the other. This fact may be associated with the similar electro negativity between Nb and Al atoms, which is 1.6 and 1.5, respectively. From this, no significant change in binding energies could be observed in XPS spectra. Based on these facts, it is possible to suggest that the behavior observed on XPS analyses is in agreement with what was observed by GAXRD analyses, towards the formation of a solid solution and reinforcing that aluminum replaces niobium atoms in the NbN lattice.

3.3 Nanohardness analysis

Mechanical behavior of as deposited thin films was verified through nanohardness tests. The hardness values obtained for samples AlN, NbN and $Nb_xAl_yN_z$ are shown in Figure 4. For AlN sample the hardness value obtained was 18.6 GPa, which has already been reported by others authors^{11,33,34}. The hardness value observed for NbN was 23.8 GPa, similar results were observed in previous works for the B1-NbN phase^{35,36}.

NbAlN_10 and NbAlN_20 samples presented similar results, varying between 25.4 and 26.3 GPa. Although these values are statistically close to NbN hardness value, it is possible to note a slight improvement, possibly due to the solid solution strengthening mechanism derived from the lattice constant shrinkage. Contrarily, the sample NbAlN_40 presented a tendency of decreasing the hardness value compared to others $Nb_xAl_yN_z$ and NbN thin films, registering a value of 22.8 GPa. This change in hardness behavior might be attributed to the growth of grain, but the amorphization observed in peak (200) previously discussed in XRD results could also slightly influence the hardness value. Indeed, according to the literature, B1-NbAlN phase

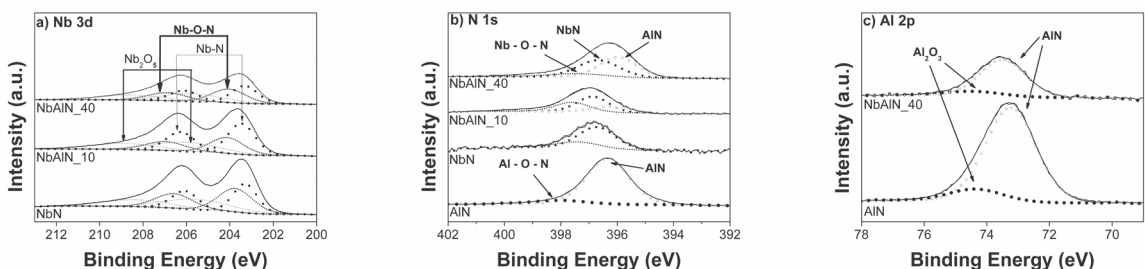


Figure 3. XPS regions for Nb 3d (a), N 1s (b) and Al 2p (c), from de NbN, AlN and $Nb_xAl_yN_z$ samples.

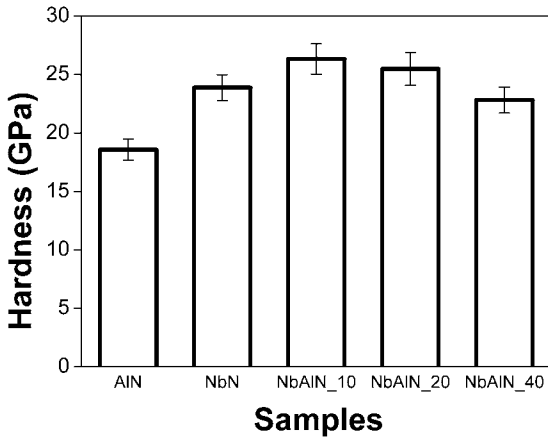


Figure 4. Hardness measurements for AIN, NbN and Nb_xAl_yN_z samples as deposited.

entirely crystalline is assumed to be the hardest phase of this ternary nitride thin films¹⁴.

The nanohardness analyses registered for NbN and Nb_xAl_yN_z coatings suggest that aluminum addition in NbN matrix for samples NbAlN_10, NbAlN_20 and NbAlN_40 does not modify significantly the coatings hardness values when compared to other Me-Al-N ternary nitrides, that show most relevant increments^{13,37,38}.

3.4 High temperature oxidation tests

Figure 5a and 5b show GAXRD results after oxidation tests at high temperatures for pure NbN and NbAlN_10 samples, respectively. For both thin films only peaks related to niobium oxide (Nb₂O₅) can be observed at 773 K (JCPDS 27 - 1312). However, in sample NbAlN_10 the Nb₂O₅ peaks are less intense compared to pure NbN, probably due to nitride/oxide structure modification. The Nb₂O₅ pattern remains at 873 K for NbN and NbAlN_10 sample. No NbN or Nb interlayer peaks can be observed, suggesting that the coatings at high temperatures were completely oxidized, from the surface to the substrate.

It is a fact that increasing the temperature further facilitates the diffusion of oxygen within the coatings. Oxidation reactions begin at the interface between the surface oxide layer and the thin film, as the amorphous layer thickens, micropores are formed on the surface, favoring oxygen diffusion. In addition, N₂ gas is released as one of the oxidation reaction products, which generates even more pores and microcracks³⁹.

Earlier works^{40,41} studied the oxidation of NbN thin films, in this case it was found that as the oxygen rate increases after oxidation at 400° C, the nitrogen concentration decreases. Nb₂O₅ formation over other oxides occurs due to the largest negative Gibbs free energy of Nb₂O₅ ($\Delta G_{1600K} = -1.215,608$ J/mol Nb) in comparison with NbO ($\Delta G_{1600K} = -277.111$ J/mol Nb) and NbO₂ ($\Delta G_{1600K} = -515,186$ J/mol Nb), showing a large difference even compared to that reported for NbN ($\Delta G_{1600K} = -85.208$ J/mol Nb) and Nb₂N ($\Delta G_{1600K} = -94.715$ J/mol Nb).

As noticed in previous works^{17,42}, in high oxidation temperatures the aluminum atoms present in the NbAlN thin films microstructure diffuses into grain boundary and surface regions, forming amorphous Al₂O₃. In Figure 3c, Al₂O₃ was detected by XPS analysis in AIN and NbAlN_40 samples as deposited, but due to its amorphous behavior, cannot be observed in the GAXRD analysis.

GAXRD results after oxidation tests at high temperatures for NbAlN_20 and NbAlN_40 samples are shown in Figure 6a and 6b, respectively. Differently from samples NbN and NbAlN_10, no relevant modification can be observed after exposure to 773 K for sample NbAlN_20. At 873 K it is possible to identify the beginning of niobium oxide formation at 22.5°. However, it is still noted the presence of small peaks related to NbN cubic phase and Nb interlayer peak, proving that the coating is not completely oxidized.

For NbAlN_40 sample, Nb₂O₅ formation was not observed in any oxidation temperature and the presence of Nb interlayer is observed even at the highest oxidation test temperature. No considerable modification can be found in

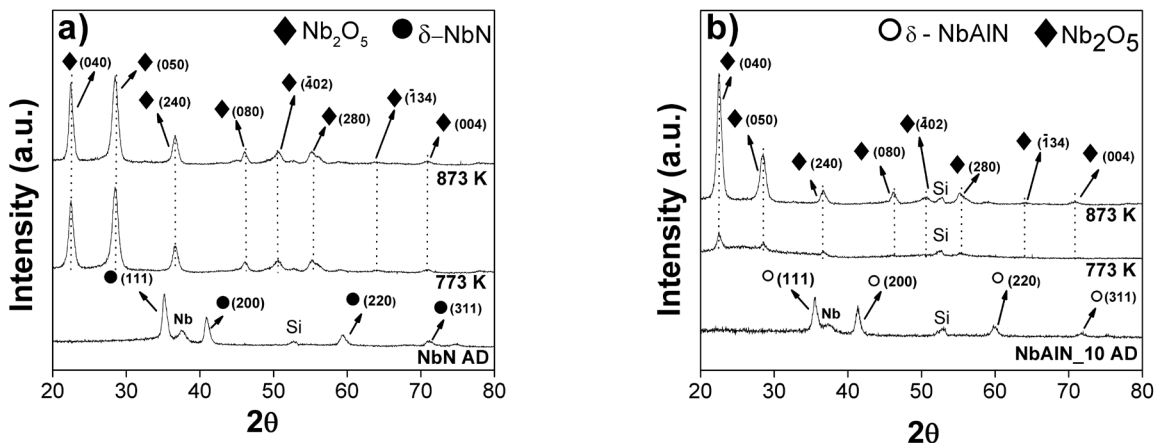


Figure 5. GAXRD patterns for (a) pure NbN and (b) NbAlN_10 sample as deposited and after oxidation tests at 773 and 873 K.

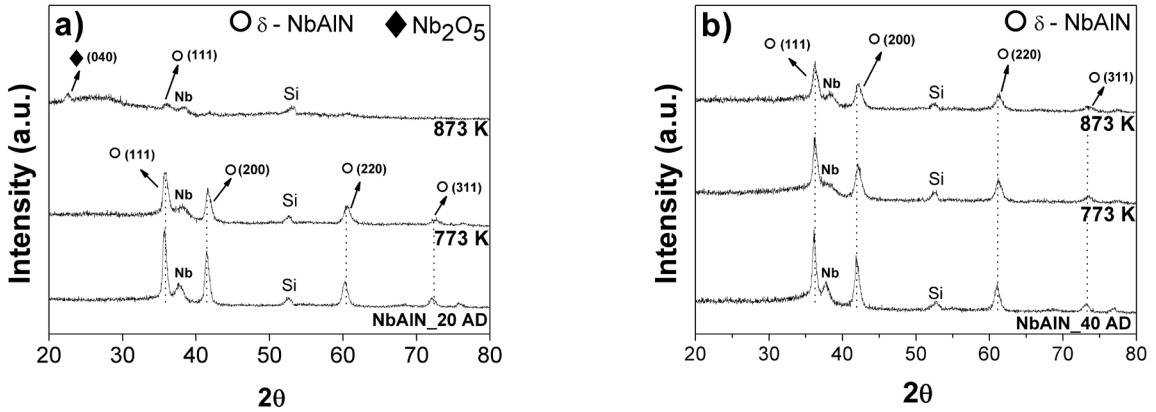


Figure 6. GAXRD patterns for (a) NbAlN_20 and (b) NbAlN_40 samples as deposited and after oxidation tests at 773 and 873 K.

XRD pattern for as deposited sample and when subjected to 873 K or lower.

The behavior of as deposited pure AlN thin film and after oxidation tests at high temperatures can be observed in Figure 7. No modification in AlN patterns or aluminum oxide formation could be found when the coatings were exposed to high temperatures. Similar results were observed earlier⁴³, proving the excellent stability at high temperatures for these coatings. Contrary to nanohardness analyses, where aluminum addition in NbN matrix did not modify significantly the $Nb_xAl_yN_z$ coatings hardness, it is possible to observe an expressive and crescent enhancement in oxidation resistance from pure NbN to NbAlN_40 sample, proving that incorporation of Al atoms in solid solution reinforce the oxidation resistance of NbN structure.

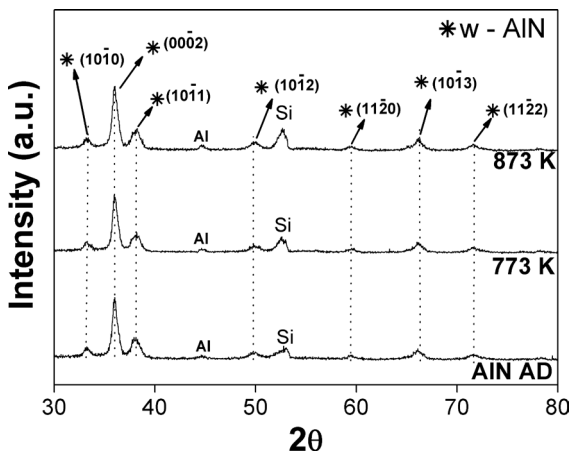


Figure 7. GAXRD patterns for pure AlN as deposited and after oxidation tests at 773 and 873 K.

3.5 Nanohardness and morphological characterization after oxidation tests

Subsequently to oxidation tests, samples were subjected surface SEM analyses and nanohardness tests in order to verify

the coatings integrity after exposure to high temperatures. AlN, NbN, NbAlN_10 and NbAlN_20 coatings showed a drastic reduction in hardness values when exposed to 873 K. Coincidentally, these samples presented a hardness value near to 9 GPa, similar to those found for silicon wafer used as substrate. On the other hand, sample NbAlN_40 presented a higher value of 17 GPa, registering a reduction of 20% in relation to the as deposited coating.

Aiming to better elucidate the reduction in coatings hardness after oxidation tests, surface SEM analyses were carried out. All studied as deposited samples presented a regular aspect, without cracks, bubbles or visible defects (not shown).

Figure 8a presents the result for sample AlN after 873 K. It is possible to verify the appearance of many cracks on the sample surface as the oxidation temperature was increased. Thus, although AlN thin films exhibit good resistance to oxidation when exposed to high temperatures (Figure 7), it showed thermal fragile characteristics probably due to cooling from 873 K to ambient temperature, justifying the loss in hardness.

SEM images obtained from NbN, NbAlN_10, NbAlN_20 and NbAlN_40 samples show comparable results. NbN and NbAlN_10 coatings after oxidation at 773 K already presented the formation of erupted bubbles on the material surface, as showed in Figure 8b and Figure 8c for samples NbN and NbAlN_10, respectively. Such fact is attributed to nitrogen gas release after the transformation of NbN into Nb_2O_5 by oxidation reactions. Nitrogen molecules formation can lead to the rupture of bubbles, allowing exposure of the substrate. Samples NbAlN_20 and NbAlN_40 also present bubbles, but none burst. In this context, such surface defects along with regions where the substrate was exposed have a direct influence on the hardness values measurement obtained for these samples.

For sample NbAlN_40, despite the maintenance of the NbN cubic phase verified in the GAXRD analysis, it was possible to verify some concentration of defects, represented

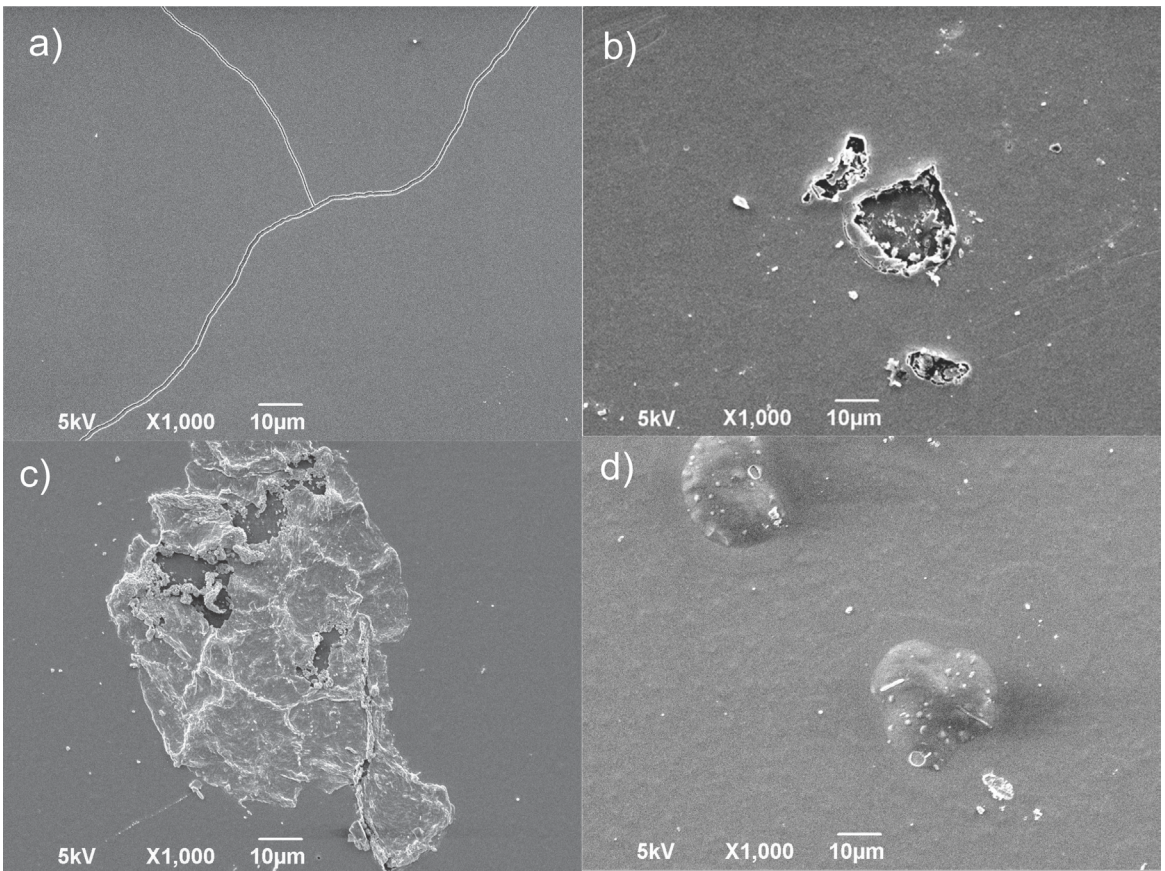


Figure 8. Surface SEM images after oxidation tests (a) AlN at 873 K; (b) NbN at 773 K; (c) NbAlN₁₀ at 773 K and (d) NbAlN₄₀ at 873 K.

by the white agglomerates (Figure 8d). However, they are in lower concentration when compared to other samples. Presence of agglomerates may be caused by the onset of oxide formation on the surface, explaining the reduction in hardness value verified after the oxidation test for this sample. Nevertheless, substrate exposure is not observed, being possible to conclude that NbAlN₄₀ sample still presents significant value compared to the literature¹⁵, showing the best results observed with GAXRD and nanohardness tests. Nonetheless, SEM analyses prove the coating integrity was not maintained after 873 K.

4. Conclusions

The influence of aluminum concentration in $Nb_xAl_yN_z$ solid solution thin films was studied in this work. From GAXRD results it was possible to observe that aluminum addition in the thin films did not change the B1-NbN phase observed in pure NbN. However, peak shifts to larger angles were observed, indicating the shrinkage of lattice constant and the formation of a solid solution, hypotheses ratified by XPS analyses. Nanohardness analyses suggest no significant modification in hardness values among NbN and $Nb_xAl_yN_z$ coatings. On the other hand, GAXRD analyses of oxidized

samples showed that aluminum addition improves substantially the oxidation resistance at high temperatures, with further increments as Al content was gradually raised in $Nb_xAl_yN_z$ coatings. Samples AlN, NbN, NbAlN₁₀ and NbAlN₂₀ after oxidation tests present hardness values identical to the silicon wafer, suggesting the substrate was exposed, what was confirmed by surface SEM analysis. The images reveal the presence of cracks and bubbles in all coatings. However, GAXRD showed that NbAlN₄₀ presented the best results against oxidation at high temperatures while hardness value was less affected.

5. Acknowledgements

The authors thank the UFRGS Ionic Implantation Laboratory for RBS analyses and CENANO-INT-RJ for XPS analyses. This work was supported by CNPQ, CAPES and FAPITEC/SE.

6. References

1. Fenker M, Balzer M, Büchi R, Jehn H, Kappl H, Lee JJ. Deposition of NbN thin films onto high-speed steel using reactive magnetron sputtering for corrosion protective applications. *Surface and Coatings Technology*. 2003;163-164:169-75.

2. Cansever N, Danisman M, Kazmanli K. The effect of nitrogen pressure on cathodic arc deposited NbN thin films. *Surface and Coatings Technology*. 2008;202(24):5919-23.
3. Rutherford KL, Hatto PW, Davies C, Hutchings IM. Abrasive wear resistance of TiN/NbN multi-layers: measurement and neural network modelling. *Surface and Coatings Technology*. 1996;86-87(Pt 2):472-9.
4. Selinder T, Sjöstrand ME, Nordin M, Larsson M, Östlund Å, Hogmark S. Performance of PVD TiN/TaN and TiN/NbN superlattice coated cemented carbide tools in stainless steel machining. *Surface and Coatings Technology*. 1998;105(1):51-5.
5. Hultman L, Engström C, Odén M. Mechanical and thermal stability of TiN/NbN superlattice thin films. *Surface and Coatings Technology*. 2000;133-134:227-33.
6. Barshilia HC, Rajam KS, Jain A, Gopinadhan K, Chaudhary S. A comparative study on the structure and properties of nanolayered TiN/NbN and TiAlN/TiN multilayer coatings prepared by reactive direct current magnetron sputtering. *Thin Solid Films*. 2006;503:158-66.
7. Paldey S, Deevi S. Single layer and multilayer wear resistant coatings of (Ti,Al)N: a review. *Materials Science and Engineering: A*. 2003;342(1-2):58-79.
8. Wang YX, Zhang S, Lee JW, Lew WS, Li B. Influence of bias voltage on the hardness and toughness of CrAlN coatings via magnetron sputtering. *Surface and Coatings Technology*. 2012;206:5103-7.
9. Badini C, Deambrosis SM, Ostrovskaya O, Zin V, Padovano E, Miorin E, et al. Cyclic oxidation in burner rig of TiAlN coating deposited on Ti-48Al-2Cr-2Nb by reactive HiPIMS. *Ceramics International*. 2017;43(7):5417-26.
10. Cai F, Chen M, Li M, Zhang S. Influence of negative bias voltage on microstructure and property of Al-Ti-N films deposited by multi-arc ion plating. *Ceramics International*. 2017;43(4):3774-83.
11. Jose F, Ramaseshan R, Balamurugan AK, Dash S, Tyagi AK, Raj B. Continuous multi cycle nanoindentation studies on compositionally graded Ti1-xAlxN multilayer thin films. *Materials Science and Engineering: A*. 2011;528(21):6438-44.
12. Boiko VI, Valyaev AN, Pogrebnjak AD. Metal modification by high-power pulsed particle beams. *Uspekhi Fiz Nauk*. 2008;169:1243-71.
13. Li D, Chen J, Zou C, Ma J, Li P, Li Y. Effects of Al concentrations on the microstructure and mechanical properties of Ti-Al-N films deposited by RF-ICPIS enhanced magnetron sputtering. *Journal of Alloys and Compounds*. 2014;609:239-43.
14. Franz R, Lechthaler M, Polzer C, Mitterer C. Structure, mechanical properties and oxidation behaviour of arc-evaporated NbAlN hard coatings. *Surface and Coatings Technology*. 2010;204(15):2447-53.
15. Benkahoul M, Zayed MK, Sandu CS, Martinu L, Klemberg-Sapieha JE. Structural, tribo-mechanical, and thermal properties of NbAlN coatings with various Al contents deposited by DC reactive magnetron sputtering. *Surface and Coatings Technology*. 2017;331:172-8.
16. Franz R, Lechthaler M, Polcik P, Figueiredo MR, Mitterer C. Tribological properties of arc-evaporated NbAlN hard coatings. *Tribology Letters*. 2012;45(1):143-52.
17. Barshilia HC, Deepthi B, Rajam KS, Bhatti KP, Chaudhary S. Structure and properties of reactive direct current magnetron sputtered niobium aluminum nitride coatings. *Journal of Materials Research*. 2008;23(5):1258-68.
18. Shannon RD. Revised Effective Ionic Radii and Systematic Studies of Interatomic Distances in Halides and Chalcogenides. *Acta Crystallographica*. 1976;A32:751-67.
19. Holec D, Franz R, Mayrhofer PH, Mitterer C. Structure and stability of phases within the NbN - AlN system. *Journal of Physics D Applied Physics*. 2010;43(14):145403.
20. Liu N, Dong L, Jin S, Wan R, Gu H, Li D. Significant impact of individual surface and modulation structure on mechanical properties of NbN/NbB2 multilayers. *Journal of Alloys and Compounds*. 2017;695:3225-32.
21. Pogrebnjak AD, Bondar OV, Abadias G, Ivashchenko V, Sobol O V, Jurga S, et al. Structural and mechanical properties of NbN and Nb-Si-N films: Experiment and molecular dynamics simulations. *Ceramics International*. 2016;42(10):11743-56.
22. Ufuktepe Y, Farha AH, Kimura S, Hajiri T, Karadag F, Al Mamun MA, et al. Structural, electronic, and mechanical properties of niobium nitride prepared by thermal diffusion in nitrogen. *Materials Chemistry and Physics*. 2013;141(1):393-400.
23. Alfonso JE, Buitrago J, Torres J, Santos B, Marco JF. Crystallographic structure and surface composition of NbNx thin films grown by RF magnetron sputtering. *Microelectronics Journal*. 2008;39(11):1327-8.
24. Ermolieff A, Girard M, Raoul C, Bertrand C, Duc TM. An XPS comparative study on thermal oxide barrier formation on Nb and NbN thin films. *Applied of Surface Science*. 1985;21(1-4):65-79.
25. Ivashchenko VI, Dub SN, Scrynskii PL, Pogrebnjak AD, Sobol' OV, Tolmacheva GN, et al. Nb-Al-N thin films: Structural transition from nanocrystalline solid solution nc-(Nb,Al)N into nanocomposite nc-(Nb, Al)N/a-AlN. *Journal of Superhard Materials*. 2016;38(2):103-13.
26. Ozgit C, Donmez I, Alevli M, Biyikli N. Self-limiting low-temperature growth of crystalline AlN thin films by plasma-enhanced atomic layer deposition. *Thin Solid Films*. 2012;520(7):2750-5.
27. Wei Q, Zhang X, Liu D, Li J, Zhou K, Zhang D, et al. Effects of sputtering pressure on nanostructure and nanomechanical properties of AlN films prepared by RF reactive sputtering. *Transactions of Nonferrous Metals Society of China*. 2014;24(9):2845-55.
28. Delpeux S, Beguin F, Benoit R, Erre R, Manolova N, Rashkov I. Fullerene core star-like polymers-1. Preparation from fullerenes and monoazidopolyethers. *European Polymer Journal*. 1998;34(7):905-15.
29. Park MH, Kim SH. Thermal conductivity of AlN thin films deposited by RF magnetron sputtering. *Materials Science in Semiconductor Processing*. 2012;15(1):6-10.

30. Ivashchenko VI, Scrynskyy PL, Lytvyn OS, Butenko OO, Sinelnichenko OK, Gorb L, et al. Comparative investigation of NbN and Nb-Si-N films: Experiment and theory. *Journal of Superhard Materials*. 2014;36(6):381-92.
31. Motamedi P, Cadien K. XPS analysis of AlN thin films deposited by plasma enhanced atomic layer deposition. *Applied Surface Science*. 2014;315(1):104-9.
32. Milošev I, Kosec T, Strehblow HH. XPS and EIS study of the passive film formed on orthopaedic Ti-6Al-7Nb alloy in Hank's physiological solution. *Electrochimica Acta*. 2008;53(9):3547-58.
33. Panda P, Ramaseshan R. Effects of Cr doping on the mechanical properties of AlN films grown by the co-sputtering technique. *Ceramics International*. 2018;45(2)(Pt A):1755-60.
34. Li W, Zhang K, Liu P, Zheng W, Ma F, Chen X, et al. Microstructural characterization and strengthening mechanism of AlN / Y nanocomposite and nanomultilayered films. *Journal of Alloys and Compounds*. 2018;732:414-21.
35. Benkahoul M, Martinez E, Karimi A, Sanjinés R, Lévy F. Structural and mechanical properties of sputtered cubic and hexagonal NbN_z thin films. *Surface and Coatings Technology*. 2004;180-181:178-83.
36. Fontalvo GA, Terziyska V, Mitterer C. High-temperature tribological behaviour of sputtered NbN_x thin films. *Surface and Coatings Technology*. 2007;202(4-7):1017-22.
37. Wang L, Zhang G, Wood RJK, Wang SC, Xue Q. Fabrication of CrAlN nanocomposite films with high hardness and excellent anti-wear performance for gear application. *Surface and Coatings Technology*. 2010;204(21-22):3517-24.
38. Xiao X, Yao B. Structure and oxidation resistance of W_{1-x}Al_xN composite films. *Transactions of Nonferrous Metals Society of China*. 2017;27(5):1063-70.
39. Frankenthal RP, Siconolfi DJ, Sinclair WR, Bacon DD. Thermal Oxidation of Niobium Nitride Films at Temperatures from 20°-400°C. *Journal of the Electrochemical Society*. 2006;130(10):2056-60.
40. Gallagher PK, Sinclair WR, Bacon DD, Kammlott GW. Oxidation of Sputtered Niobium Nitride Films. *Journal of the Electrochemical Society*. 2006;130(10):2054-56.
41. Oliveira RM, Hoshida L, Oliveira AC, Silva MMNF, Pichon L, Santos NM. Evaluation of the resistance to oxidation of niobium treated by high temperature nitrogen Plasma Based Ion Implantation. *Surface and Coatings Technology*. 2017;312:110-6.
42. Ichimura H, Kawana A. High-temperature oxidation of ion-plated TiN and TiAlN films. *Journal of Materials Research*. 1993;8(5):1093-100.
43. Kar JP, Bose G, Tuli S. Influence of rapid thermal annealing on morphological and electrical properties of RF sputtered AlN films. *Materials Science in Semiconductor Processing*. 2005;8(6):646-51.